Journal of Power Sources 194 (2009) 991–996

Contents lists available at ScienceDirect

Journal of Power Sources

journal homepage: www.elsevier.com/locate/jpowsour

Short communication

Control of variable power conditions for a membraneless direct methanol fuel cell

Alfred Lam[a,b], David P. Wilkinson[a,b,*], Jiujun Zhang[a,b]

[a] Department of Chemical and Biological Engineering, University of British Columbia, 2360 East Mall, Vancouver, BC, Canada V6T 1Z4
[b] Institute for Fuel Cell Innovation, National Research Council Canada, 4250 Wesbrook Mall, Vancouver, BC, Canada V6T 1W5

ARTICLE INFO

Article history:
Received 24 April 2009
Received in revised form 21 May 2009
Accepted 22 May 2009
Available online 30 May 2009

Keywords:
Direct methanol fuel cell
Membraneless fuel cell
Power control
Guard

ABSTRACT

The control of a direct methanol fuel cell (DMFC) operating under variable power conditions is important in the development of a commercially applicable device. Fuel cells are conventionally designed for a maximum power output. However variable load cycles can result in fuel cell operation under sub-optimal conditions. In this paper, a simple method of power management using a physical guard is presented. The guard can be used on the anode or cathode electrode, in the membraneless gap or in any combination. This design selectively deactivates specific active regions of the electrode assembly and enables the DMFC to operate at a constant voltage and current density at different absolute power conditions. The guard also serves to control excessive crossover during shutdown and low power operation.

1. Introduction

A common challenge for a conventional direct methanol fuel cell (DMFC) is the ability to manage variable load and power cycles. Fuel cells are generally designed to accommodate the peak power of a certain device but frequent changes in power requirements result in sub-optimal conditions. For instance, on a typical power curve, the power demand varies with the amount of current drawn by the device resulting in a fluctuating rate of fuel consumption over the active area. This is of specific concern at lower power levels or when the fuel cell is shutdown as the issue of crossover is magnified due to an excess concentration of methanol. In active systems, the conventional methods to address this issue are related to the balance of plant (BoP) components. A combination of sensors, pumps, and valves along with dosing and purging procedures are used to adjust the fuel concentration and stoichiometry [1–5]. For passive systems, the issue is more serious as they do not contain additional BoP components to control the fuel concentration or stoichiometry at different power levels [4].

In this paper, a simple method of power management using a physical guard for a membraneless DMFC is presented. The novel membraneless architecture has been demonstrated in a previous study by the authors [6] and involves the replacement of the polymer electrolyte membrane (PEM) by an open spacer with a liquid electrolyte (i.e., 0.5 M H_2SO_4) providing the proton conduction, as shown in Fig. 1. This novel arrangement is coupled with an electrolytic fuel for ionic conduction and addresses several key limitations with the membrane such as finite proton conductivity, dehydration, degradation and poisoning effects. To control the power of the membraneless DMFC, a physical guard is used to selectively deactivate/activate specific regions of the electrode assembly. It can be placed either on the anode, within the open spacer, or on the cathode as shown in Fig. 2a–c or any combination of (a) to (c) to create an effective active area as shown in Fig. 3. The theory of the triple phase boundary (TPB) is the fundamental concept behind the design. This theory states that an electrochemical reaction can only occur at a TPB site where the electrolyte, reactants and an electrically connected catalyst are in contact [7]. If the contact of these components can be controlled, certain portions of the area of an electrode can be deactivated or activated. For approaches where the anode and/or cathode area is covered, deactivation occurs through the restriction of the reactant and/or electrolyte (for example, methanol, oxygen, acid, etc.) to the catalyst sites. For approaches where the open spacer is blocked, deactivation occurs by limiting or severing the ionic contact between the anode and cathode. The contribution to the total power output is controlled by the limited reactivity of these regions.

* Corresponding author at: Department of Chemical and Biological Engineering, University of British Columbia, 2360 East Mall, Vancouver, BC, Canada V6T 1Z4.
E-mail address: dwilkinson@chml.ubc.ca (D.P. Wilkinson).

0378-7753/$ – see front matter © 2009 Elsevier B.V. All rights reserved.
doi:10.1016/j.jpowsour.2009.05.038

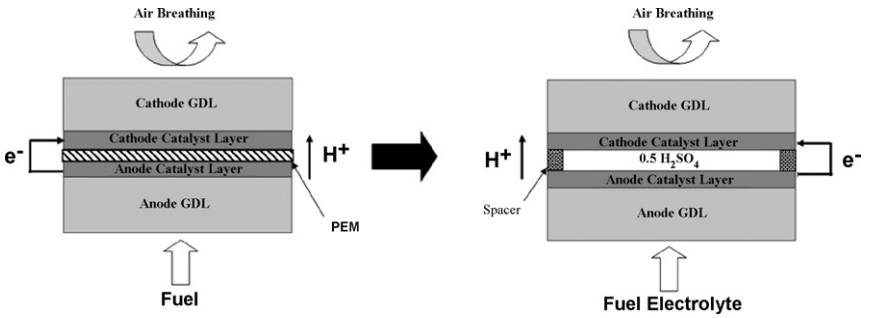

Fig. 1. Schematic of a conventional membrane electrode assembly (MEA) and a membraneless electrode assembly.

2. Materials and methods

2.1. Electrode assembly preparation

Perforated graphitic foil with a 4.95% open area, supplied by GrafTech International Ltd., was cut into samples with a 25 mm diameter for use as a current collector on the anode side. The electrodes were prepared by a spray deposition method using an AccuSpray spray gun. For both the anode and cathode electrodes, Etek-TGPH-060 carbon fibre paper with 20% wet proofing was used. On the anode, a loading of 4.00 mg cm^{-2} carbon supported (Vulcan XC-72) 40 wt% Pt–Ru (1:1 atomic ratio, or a/o) catalyst with a Nafion® loading of 30 wt% was applied. On the cathode, a loading of 1.36 mg cm^{-2} carbon supported (Vulcan XC-72) 20 wt% Pt catalyst with a Nafion® loading of 30 wt% and a 1.00 mg cm^{-2} Cabot carbon sublayer with 20 wt% PTFE was applied. From a 11 cm × 11 cm electrode, smaller samples with a diameter of 16.5 mm were cut out for the electrode assembly holder. The membraneless open spacer was made with Dow Corning Siliastic J-RTV silicone rubber and a curing agent. The spacer had an outer diameter of 25 mm and an inner diameter of 16 mm with thickness of 0.5 mm.

2.2. Guard preparation for open spacer and electrode coverage

Sheets of Kapton® 100JP from DuPont or Millipore hydrophobic filter paper were cut into circular shapes and were used as the materials for the physical guard. For the purpose of a simple demonstration of various power levels, the circular guards were further cut into 25%, 50% and 75% of the total open area.

2.3. Fuel cell performance testing

The electrode assembly with the physical guard was incorporated into an electrode assembly holder with a 2.0 cm^2 active area. The performance of the air breathing membraneless DMFC was recorded at ambient temperature and pressure (25 °C, 1 atm) with a single chamber glass cell as shown in Fig. 4. In the fuel cell testing an aqueous fuel/electrolyte solution (5 M CH_3OH + 0.5 M H_2SO_4) was used. Polarization curves were obtained using a Solartron 1420E Multistat operated in galvanostatic mode. The specific electrode potentials were monitored with a double junction saturated calomel electrode (SCE) located in the anodic chamber.

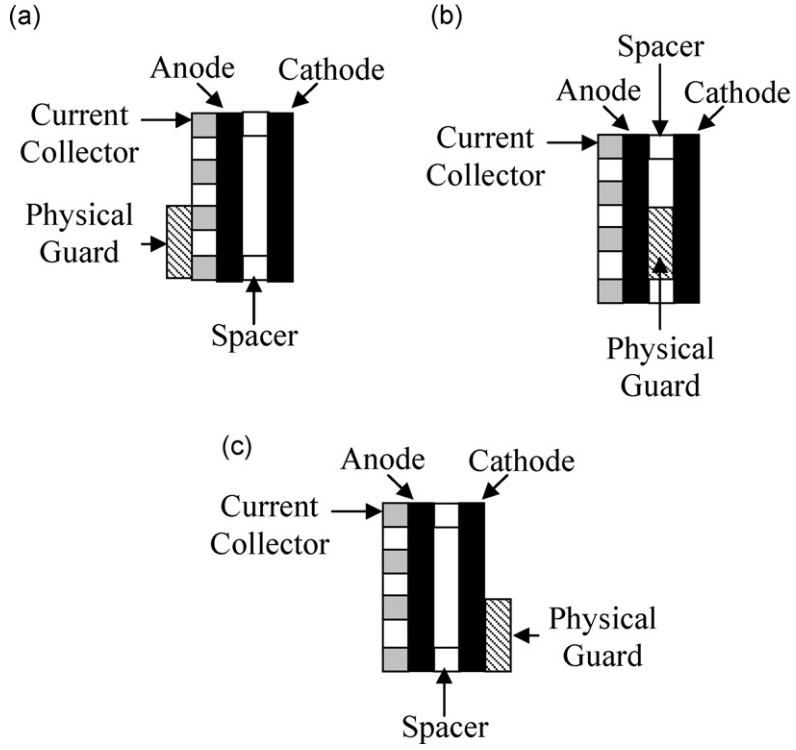

Fig. 2. Profile view of a membraneless electrode assembly with a physical guard (a) on the anode side, (b) within the open area of the spacer, and (c) on the cathode side.

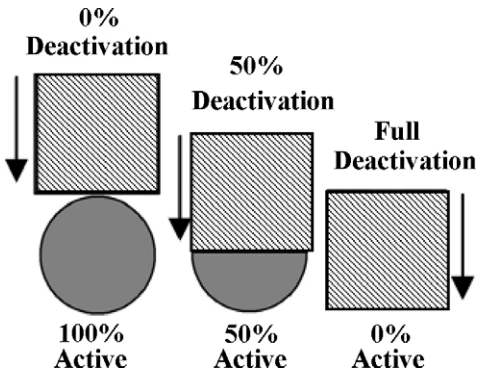

Fig. 3. Schematic of the effective active area created by a physical guard. The covered area is deactivated.

2.4. Passive fuel crossover

The fuel crossover was tested under passive conditions (i.e., no load) at ambient temperature and pressure with a two-chamber glass diffusion cell. A 5 M methanol bulk solution was initially introduced into the donor chamber and 18 MΩ water into the receptor chamber. The changes in methanol concentration of the receptor chamber was monitored by circulating its contents through a Waters 2414 Refractive Index detector. The perforated current collector and the anode electrode was incorporated into an electrode assembly holder with a 2.0 cm^2 active area and clamped between the two chambers. For the demonstration of crossover with different active areas, Kapton® 100JP guards were implemented at 25%, 50% and 75% of the total open area on the anode side.

3. Results and discussion

Shown in Fig. 5a are the performance and power curves, on an absolute current basis, for a membraneless DMFC with a guard positioned within the open spacer. In the segmented section, the anode and cathode are deactivated through ionic isolation. An important aspect to note is that at any specified power level, the voltage remains constant. This is in stark contrast to conventional fuel cell configurations where the voltage fluctuates along the power curve at different load conditions. Advantages of a constant voltage include the elimination of damage to electrical components due to large voltage surges, higher DC–DC converter (voltage regulator) efficiency due to closely matched input/output voltages [8], easier detection of failure modes (e.g., possible failure if the voltage of

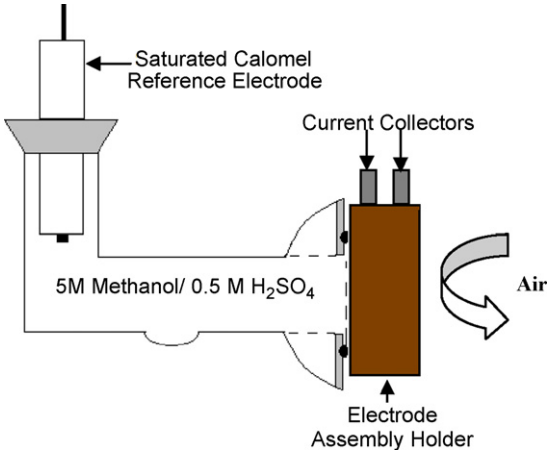

Fig. 4. Schematic of 2.0 cm^2 passive air breathing glass cell used for performance testing.

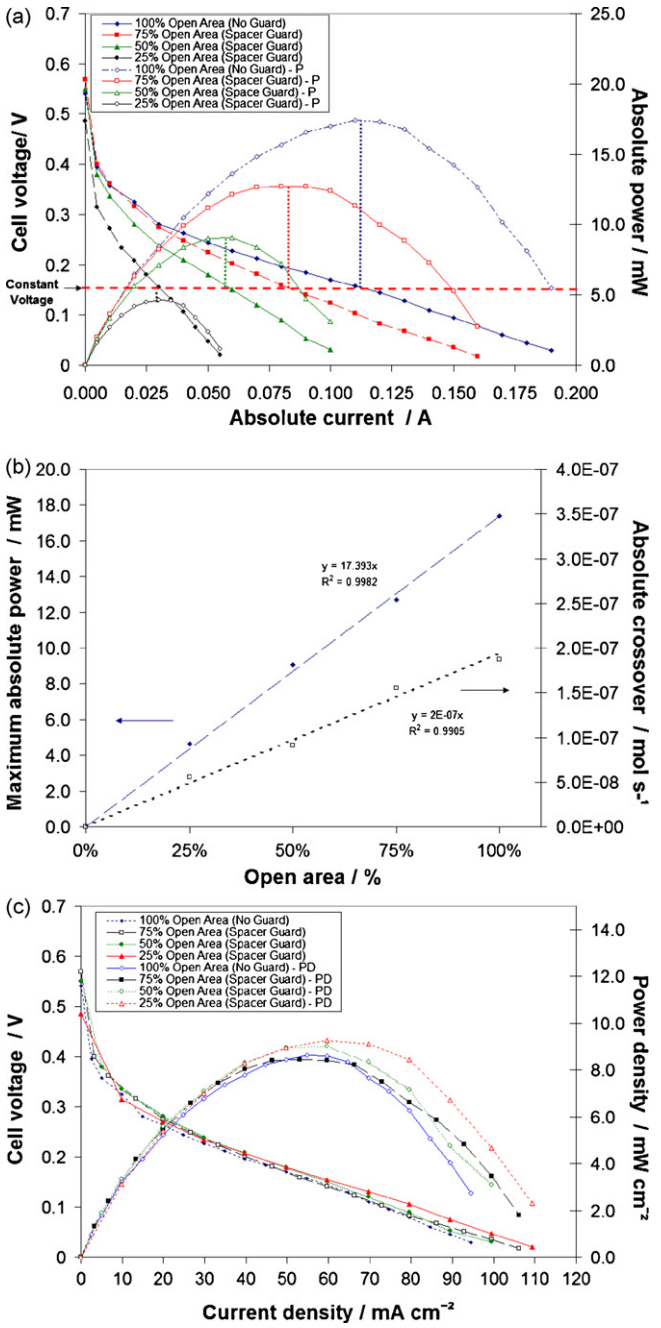

Fig. 5. (a) Polarization and power curves on an absolute current basis for the different effective active areas created by a guard within the open area of the spacer. (b) Relationship between absolute peak power and the absolute crossover vs. the different effective active areas created by a guard within the open area of the spacer. (c) Polarization and power curves, normalized to the effective active area, for an electrode assembly with a guard placed within the open area of the spacer.

different open areas deviates greatly from a constant value), constant voltage efficiency and less cyclic voltage degradation [9]. The direct proportionality of absolute power and the effective active area shown in Fig. 5b, demonstrates the effectiveness of the guard in controlling the power output. Similarly the guard is effective in controlling the fuel crossover.

The absolute performance of the membraneless DMFC normalized to an effective open area is shown in Fig. 5c. The similarity in polarization and power curves indicates that the performance remains constant over the entire effective area of the electrode assembly. The peak power density occurs at a constant current den-

sity value of ~55–60 mA cm^{-2} regardless of the open area. Unlike conventional fuel cell configurations where the consumption rate varies with the load cycle, the advantage of a fuel cell operating with a guard is that it can be designed to operate at a single optimal point where the fuel consumption per unit area (mol cm^{-2} s^{-1}) is constant. This is particularly important in the operation of a passive fuel cell where BoP components are unavailable to actively control the fuel concentration and stoichiometry. Furthermore, the guard also serves to prevent excessive fuel crossover at low power levels or when the fuel cell is shutdown. This has significant advantages over conventional designs because crossover can now be controlled and is no longer variable on a normalized area basis. This can be seen from the general flux equation of methanol ($J_{CH_3OH,m}$/mol cm^{-2} s^{-1}) with the assumption of negligible pressure differential between the anode and cathode. It is defined as a combination of the electro-osmotic drag component, related to the number of solvated methanol molecules around each proton ($\omega_{CH,OH}$) and the diffusive component, which is related to the diffusion coefficient (D_{CH_3OH}/cm^2 s^{-1}) and the concentration gradient ($C_{CH_3OH,a} - C_{CH_3OH,c}$/mol cm^{-3}) across the spacer thickness (τ/cm) as shown in Eq. (1). In this equation, the flux towards the cathode is considered negative:

$$J_{CH_3OH,m} = \omega_{CH_3OH} N_{H^+} - D_{CH_3OH}\left(\frac{C_{CH_3OH,a} - C_{CH_3OH,c}}{\tau}\right) \quad (1)$$

At low power levels the diffusive component is dominant as fewer protons are produced and conducted to the cathode. Shown in Fig. 5b, is the direct proportionality between the % open area and the absolute fuel crossover. When normalized to the effective area this value remains stable at each power level. Due to a fixed consumption per unit area and flux of protons (N_{H^+}/mol cm^{-2} s^{-1}), the interfacial concentration at the anode/spacer interface can be maintained leading to a constant methanol flux. During shutdown the guard can be completely closed to prevent any methanol from crossing over to the cathode.

In addition, operating at constant conditions has significant advantages over conventional DMFCs as the design is considerably simplified. This is especially true when optimizing a fuel cell for a targeted energy density. This metric is important when comparing fuel cells with a conventional rechargeable battery. A state of the art Li-ion battery has a volumetric energy density of ~350 Wh L^{-1} and a gravimetric energy density of ~150 Wh kg^{-1} [10] and in order for the DMFC to compete commercially, higher energy density is required. Although neat methanol at standard conditions (25 °C, 1 atm) has a volumetric and gravimetric energy density of 4820 Wh L^{-1} [4] and 6124 Wh kg^{-1}, respectively, an overall efficiency >7.26% on a fuel basis is necessary to achieve a volumetric energy density similar to the Li-ion battery. However under practical conditions, the overall efficiency must be even higher as the fuel dilution must also be taken into account. The overall fuel cell efficiency ($\eta_{overall}$) is defined by the relationship shown in Eq. (2) [11]:

$$\eta_{overall} = \eta_v \times \eta_f = \left(\frac{E_{cell}}{E_{tn}}\right)\left(\frac{i}{i + i_{crossover}}\right) \quad (2)$$

The voltage efficiency (η_v) is a function of the actual cell voltage (E_{cell}) and theoretical maximum voltage (E_{tn}), and the Faradaic efficiency (η_f) is a function of the current density (i/A cm^{-2}) and crossover current density ($i_{crossover}$/A cm^{-2}). With conventional fuel cells, constant variations in efficiency arises from changes in cell voltages (E_{cell}/V) and the crossover ($i_{crossover}$/A cm^{-2}) at different power demands. With the implementation of the guard to control the effective active area, the voltage and crossover are approximately constant at different power levels thus making the efficiency stable at different power levels.

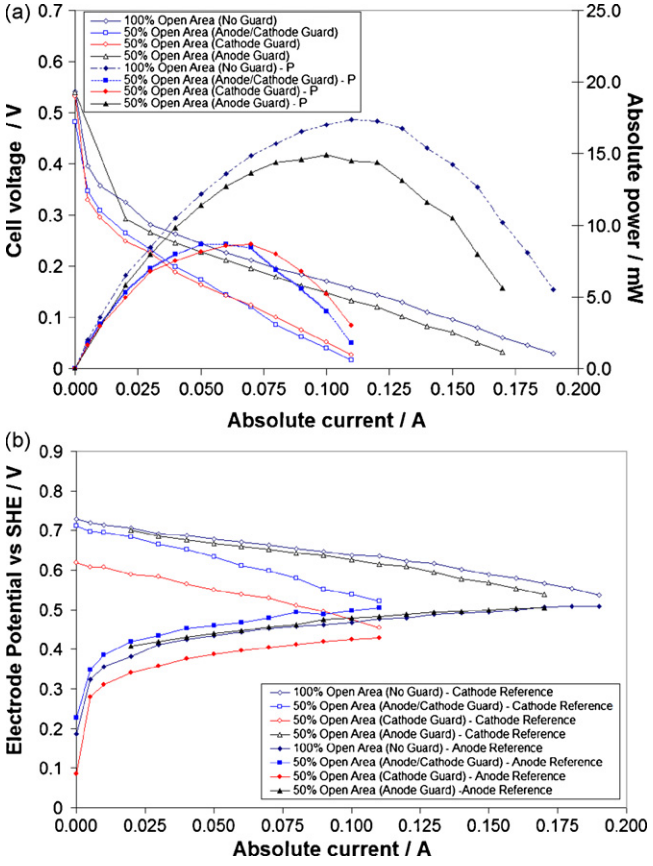

Fig. 6. (a) Polarization and power curves on an absolute current basis for the cases where a guard deactivates 50% of the anode or cathode or both the anode/cathode as compared to a baseline case without a guard. (b) Electrode potentials on an absolute current basis for cases where a guard deactivates 50% of the anode or cathode or both the anode/cathode as compared to a baseline case without a guard.

To examine the effectiveness of other guard configurations where the anode (Fig. 2a), the cathode (Fig. 2b) and a combination of the anode and cathode are covered, the absolute performance at a 50% effective area was plotted versus a baseline case with 100% open area and is shown in Fig. 6a. All arrangements, with the exception of the case where only the anode was covered, resulted in a reduction of absolute power of ~50%. In this case, the individual electrode potentials, shown in Fig. 6b, revealed that there was minimal deactivation. The electrode potentials for the anode guard were similar to the baseline case over the absolute current range. To help qualitatively explain this phenomenon, an equivalent circuit (Fig. 7) showing the mass transfer resistance of the electrolyte fuel solution in the electrode assembly is used. The equivalent circuit has two horizontal paths that represent the through plane diffusion resistance of the open side (R_{do}, R_{eo}, R_{so}) and the closed side (R_{dc}, R_{ec}, R_{sc}) and two vertical paths (R_{er}, R_{sr}) that represent the diffusion resistance within the electrode and spacer in the lateral direction. For the case with an open spacer, shown in Fig. 7, the electrolyte fuel is able to diffuse in the through plane direction along $R_{do} \rightarrow R_{eo} \rightarrow R_{so}$ path. Although the direct access to the catalyst sites along $R_{dc} \rightarrow R_{ec}$ path on the anode side is blocked by the guard, the majority of the sites remain active due to the lateral diffusion in the spacer. The lateral diffusion in the electrode has a less significant effect as the porous structure makes the lateral resistance R_{er} larger than that of the open spacer (R_{sr}). To improve the effectiveness of the anode guard, an increase in mass transport resistance in the lateral direction (R_{sr}) within the open spacer is necessary. This can be accomplished by substituting the open spacer with a porous material (e.g., Fisherbrand G4 Borosilicate hydrophilic glass filter paper)

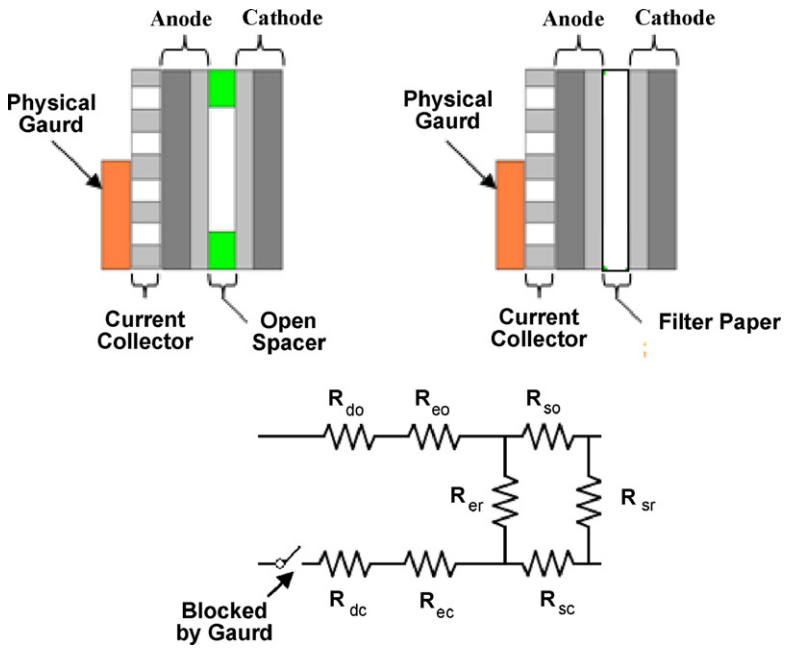

Fig. 7. Equivalent circuit for mass transfer resistance (R_i) in an electrode assembly with a lateral diffusion barrier and a guard on the anode (R_{do} = diffusion barrier resistance open side; R_{dc} = diffusion barrier resistance closed side; R_{eo} = electrode resistance open side; R_{ec} = electrode resistance closed side; R_{so} = spacer resistance open side; R_{sc} = spacer resistance closed side; R_{er} = electrode resistance in lateral direction; R_{sr} = separator resistance in lateral direction).

as shown in Fig. 7. The lateral mass transfer resistance (R_{sr}/cm^{-1} s) is the inverse of the lateral mass transfer coefficient (K_{sr}/cm s^{-1}) and is a function of the effective diffusion coefficient ($D_{eff,sr}$/cm^2 s^{-1}) and the distance in the lateral direction (L/cm). In porous media where a solute is diffusing through fluid filled pores, the effective diffusion coefficient is dependent on the diffusion coefficient in the pores (D/cm^2 s^{-1}), the porosity (ε) and the actual pore length per distance (a) in the direction of diffusion [12]. To increase the lateral mass transfer resistance, R_{sr}, the parameters shown in Eq. (3) can be modified (e.g., decrease porosity, etc.)

$$R_{sr} = \left(\frac{1}{K_{sr}}\right) = \left(\frac{L}{D_{eff,sr}}\right) = L\left(\frac{a^2}{D \cdot \varepsilon}\right) \quad (3)$$

Fig. 8 showed that the implementation of the lateral diffusion media improved the effectiveness of the anode guard in reducing the absolute power by ~50%. Although there are benefits to the use of the filter paper with the anodic guard, under practical conditions a substantially open area would be preferred as the ohmic resistance would be lower.

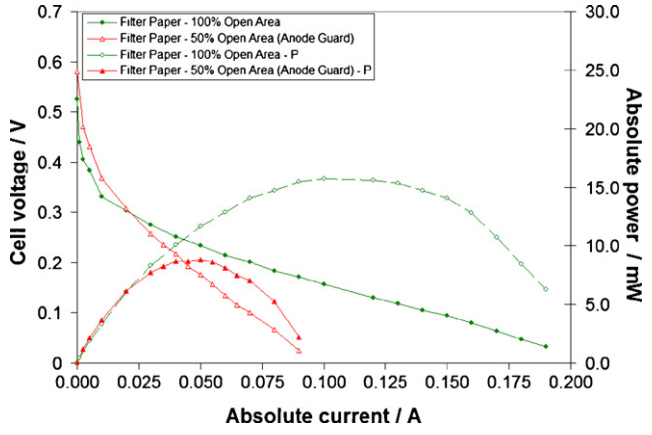

Fig. 8. Polarization and power curves on an absolute current basis for an electrode assembly with a lateral diffusion barrier (filter paper spacer) and a guard covering 50% of the anode.

Furthermore, the other configurations in Fig. 6a (i.e., cathode or anode/cathode coverage) also experience the lateral transport of the electrolyte fuel within the open spacer. However, the reason this approach is effective is because the primary mechanism of deactivation is attributed to the oxidant being restricted at the cathode. The lateral transport of oxygen in the open spacer is not considered as significant since the rate of diffusion of gas in a liquid is slow therefore the cathode catalyst sites remain inactive. A larger active area would also be expected to limit lateral diffusion as the distance from open and blocked regions are extended.

To show the actual operation under an active load cycle, a manually operated guard on the cathode was employed. The load was cycled for 5 min each at 0.03 A (50% open area), 0.06 A (100% open area) and back to 0.03 A (50% open area) with an 8-s interval in between currents at open circuit to allow for the manual positioning of the guard. Fig. 9 shows that the electrode assembly was effectively deactivated and activated to control the total power output at a 50% power condition of ~6.7 mW and a 100% power condition of ~13.7 mW while maintaining a constant voltage of ~0.215 V.

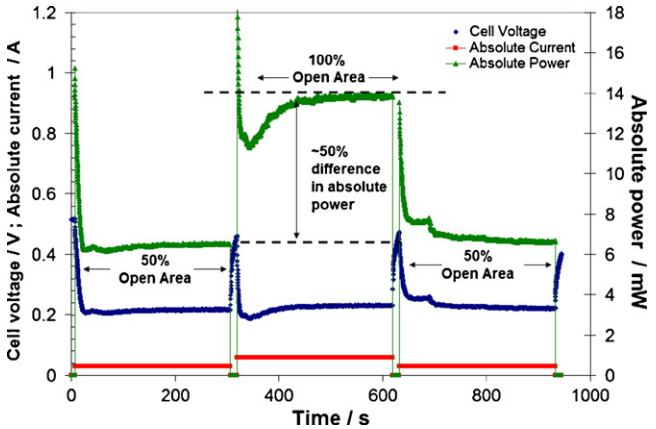

Fig. 9. Membraneless DMFC operating under a varying load cycle with a manually positioned guard on the cathode.

4. Conclusions

A simple method to control the total power output of a membraneless DMFC has been demonstrated by selectively disrupting the triple phase regions with a physical guard on or within the electrode assembly. This allows for the operation of the membraneless DMFC at a single operating condition (i.e., constant voltage, fuel consumption and crossover) with a constant overall efficiency and areal power density. This approach has significant advantages as the design, control and optimization are considerably simplified over conventional DMFCs. This control method may be especially useful for passive systems where the control of fuel concentration or stoichiometry is difficult. The optimal configurations have the characteristics of effective power control and control of fuel crossover at low power and shutdown conditions. The preferred placement of the guard when a lateral diffusion media is not present is within the open spacer. When the lateral diffusion barrier is present, the preferred arrangement is the placement of the guard on the anode. Other combinations that include these two arrangements can also be effectively implemented. Although electrically insulating materials were used in this paper, electrically conductive materials can be implemented for the anode and/or cathode guard. In this way, the guard can have the dual role of current collection and power control.

Acknowledgments

Funding for this project has been provided by the National Research Council Institute for Fuel Cell Innovation (NRC-IFCI), Natural Sciences & Engineering Research Council (NSERC) and the University of British Columbia. The authors would also like to thank Dr. Brett Sharp and Dr. Paul Cyr for their valuable input and the NRC-IFCI and UBC machine shops for the fabrication of peripheral components for the test apparatus.

References

[1] Z. Qi, M. Hollett, C. He, A. Attia, A. Kaufman, Electrochem. Solid-State Lett. 6 (2003) A27–A29.
[2] R. Jiang, D. Chu, J. Power Sources 161 (2003) 1192–1197.
[3] H. Zhao, J. Shen, J.J. Zhang, H. Want, D.P. Wilkinson, C.E. Gu, J. Power Sources 159 (2006) 626–636.
[4] W. Qian, D.P. Wilkinson, J. Shen, H. Wang, J.J. Zhang, J. Power Sources 154 (2006) 202–213.
[5] D.P. Wilkinson, M. Blanco, H. Zhao, J. Wu, H. Wang, Electrochem. Solid-State Lett. 10 (2007) B155–B160.
[6] A. Lam, D.P. Wilkinson, J.J. Zhang, Electrochim. Acta 53 (2008) 6890–6898.
[7] R. O'Hayre, D.M. Barnett, F.B. Prinz, J. Electrochem. Soc. 152 (2005) A439–A444.
[8] M.H. Rashid, Power Electronics Handbook, Academic Press, 2001, p. 220.
[9] J.Y. Park, J.H. Lee, J. Sauk, I.H. Son, Int. J. Hydrogen Energy 33 (2008) 4833–4843.
[10] G. Pistoia, Batteries for Portable Devices, Elsevier, 2005, p. 79.
[11] T.S. Zhao, K.D. Kreuer, T.V. Nguyen, Advances in Fuel Cells, Elsevier, 2007, p. 203.
[12] E.L. Cussler, Diffusion – Mass transfer in fluid Systems, 2nd ed., Cambridge University Press, 1997, p. 173.